



## Full Text View

[Volume 30, Issue 5 \(May 2000\)](#)

### Journal of Physical Oceanography

Article: pp. 868–887 | [Abstract](#) | [PDF \(735K\)](#)

# Formation Mechanisms for North Pacific Central and Eastern Subtropical Mode Waters

**Carol Ladd and LuAnne Thompson**

*School of Oceanography, University of Washington, Seattle, Washington*

(Manuscript received September 4, 1998, in final form May 10, 1999)

DOI: 10.1175/1520-0485(2000)030<0868:FMFNPC>2.0.CO;2

### ABSTRACT

The effects of one-dimensional processes on the formation of deep mixed layers in the central mode water (CMW) and eastern subtropical mode water (ESMW) formation regions of the North Pacific have been analyzed using a mixed layer model. By running the model with various combinations of initial (August) background stratification and forcing fields (heat flux,  $E - P$ , and wind stress), and comparing the resultant March mixed layer depths, the relative importance of these effects on creating deep mixed layers was diagnosed. Model results suggest that the contributions of evaporation minus precipitation and wind mixing to mixed layer depth in both the CMW and the ESMW formation regions are negligible.

In the ESMW formation region (centered at approximately 30°N, 140°W), the initial stratification is very important in determining where deep mixed layers form. Summer heating is quite weak in this region, resulting in a weak (or even nonexistent) seasonal pycnocline at the end of the summer at about 30°N. It is this lack of shallow seasonal stratification that allows a local maximum of winter mixed layer depth even though the wintertime cooling is much weaker than other regions of locally deep mixed layers.

In the CMW formation region (approximately 40°N between 170°E and 160°W), in contrast to the ESMW formation region, wintertime cooling is strong enough to erode through the shallow seasonal pycnocline. In the region of deepest mixed layers in the CMW region, the deeper stratification (150–400 m) is quite weak. Once the seasonal pycnocline has been eroded away, the lack of deeper stratification becomes important in allowing the mixing to penetrate further.

#### Table of Contents:

- [Introduction](#)
- [Model](#)
- [Eastern subtropical mode](#)
- [Central mode water \(179.5°E\)](#)
- [Wind mixing and E –](#)
- [Summary and discussion](#)
- [REFERENCES](#)
- [TABLES](#)
- [FIGURES](#)

#### Options:

- [Create Reference](#)
- [Email this Article](#)
- [Add to MyArchive](#)
- [Search AMS Glossary](#)

#### Search CrossRef for:

- [Articles Citing This Article](#)

#### Search Google Scholar for:

- [Carol Ladd](#)
- [LuAnne Thompson](#)

## 1. Introduction

The link between the atmosphere and the subsurface ocean is largely dependent on processes affecting ventilation of the thermocline. When mixed layer water is detrained from the mixed layer into the thermocline, it brings with it properties (such as temperature, salinity, potential vorticity, chemical tracers) formed through interaction with the atmosphere. If this mixed layer water subducts into the *permanent* thermocline, those properties are insulated from further interaction with the atmosphere, thus modifying water properties and circulation patterns in the permanent thermocline. The formation of mode water may be an important source of low potential vorticity to the thermocline.

Mode water formation may be an important method of transmitting the effects of atmospheric forcing to the subsurface ocean. [Worthington \(1959\)](#) first recognized the importance of mode water with his study of 18° Water in the subtropical North Atlantic. Since then, mode water has also been identified in the western North Pacific ([Masuzawa 1969](#)) and South Pacific ([Roemmich and Cornuelle 1992](#)), the central North Pacific ([Nakamura 1996](#); [Suga et al. 1997](#)), and the eastern subtropical North Atlantic ([Siedler et al. 1987](#)). Most recently, [Hautala and Roemmich \(1998, hereafter HR98\)](#) have identified a region of weak mode water formation in the eastern subtropical North Pacific.

Mode water formation depends crucially on the seasonal cycle of the mixed layer. The canonical view of mode water formation begins with a large heat loss to the atmosphere during the winter resulting in a deep mixed layer. In addition to heat fluxes, wind mixing, transport convergences, and the background structure of the stratification can play a role in the formation of deep mixed layers. When the mixed layer restratifies due to heat gain during the summer, the deeper part of the winter mixed layer is detrained into the seasonal thermocline. If the mixed layer reached the same depth every winter everywhere, all of the water in the seasonal thermocline would be reentrained into the mixed layer during the succeeding winter. However, due to the temporal and spatial dependence of the depth of the late winter mixed layer, water can be subducted into the permanent thermocline by advecting along sloping isopycnals to depths deeper than the winter mixed layer. The influence of temporal and spatial variations in mixed layer depth (MLD) on subduction and the resulting impact on formation of thermocline waters has been examined by numerous investigators, including [Stommel \(1979\)](#), [Woods \(1985\)](#), [Cushman-Roisin \(1987\)](#), and [Alexander and Deser \(1995\)](#).

When a thick layer of nearly homogeneous water enters the permanent thermocline, it is called mode water. The rate of mass exchange from the mixed layer/seasonal pycnocline into the permanent pycnocline has been termed the subduction rate ([Marshall et al. 1993](#); [Huang and Qiu 1994](#); [Qiu and Huang 1995](#)). Mode water formation regions occur where the subduction rate is large.

The North Pacific subtropical mode water (STMW) is the most intensively studied mode water mass in the North Pacific. [Worthington \(1959\)](#), in his study of the North Atlantic Eighteen Degree Water, first noted the existence of a thermostad at 16.5°C in the North Pacific. [Masuzawa \(1969, 1972\)](#) later described distributions of this North Pacific variety of STMW. Masuzawa found, in a volumetric census of the subtropical gyre, a bivariate mode at 16.5°C, 34.75 psu. He also found significant thickening of isotherm spacing for the temperature range between 16° and 19°C. By defining mode water as the water mass with a vertical potential temperature gradient less than 1.5°C/100 m, [Suga et al. \(1997\)](#) estimate a characteristic temperature range of 15°–18°C. [Nakamura \(1996\)](#) estimates a temperature range of 15.5°–17.5°C and a salinity range of 34.65–34.80 psu by analyzing  $T$ - $S$  diagrams limited to parcels of water with potential vorticity (PV) less than  $1.5 \times 10^{-10} \text{ m}^{-1} \text{ s}^{-1}$ .

The North Pacific central mode water (CMW) has only recently been identified ([Nakamura 1996](#); [Suga et al. 1997](#)). The CMW pycnostad is identified by low PV on the  $\sigma_\theta = 26.2 \text{ kg m}^{-3}$  isopycnal surface in the central subtropical gyre [see [Fig. 4](#) in [Talley \(1988\)](#)]. By analyzing  $T$ - $S$  diagrams limited to parcels of water with PV less than  $1.5 \times 10^{-10} \text{ m}^{-1} \text{ s}^{-1}$ , [Nakamura \(1996\)](#) estimates characteristic potential temperature, salinity, and  $\sigma_\theta$  ranges of 8.5°–11.5°C, 34.10–34.35 psu, and 26.0–26.5  $\text{kg m}^{-3}$ , for CMW. [Suga et al. \(1997\)](#) estimates a potential temperature range of 9°–13°C.

[Talley \(1988\)](#) identifies a lateral minimum in potential vorticity in the eastern Pacific centered at approximately 30°N, 140°W. She points out that this minimum lies under a region of maximum Ekman downwelling [calculated from [Han and Lee's \(1981\)](#) wind stress analysis]. HR98 study this potential vorticity minimum in more detail and identify it as eastern subtropical mode water (ESMW), a mode water mass distinct from both the western subtropical mode water ([Masuzawa 1969](#)) and the central mode water ([Nakamura 1996](#); [Suga et al. 1997](#)).

Because the CMW and the ESMW have only recently been identified, they have not been very thoroughly studied as yet. The above referenced studies primarily concentrated on identifying the water properties and circulation of the mode water masses. [Suga et al. \(1997\)](#) and [Nakamura \(1996\)](#) estimate a formation region for the CMW, but the region is probably not as well defined as it could be and the formation mechanisms have not been thoroughly studied. Formation mechanisms are particularly unclear for the ESMW because the heat fluxes are not as strong in the ESMW formation region as in the STMW

and CMW formation regions (Fig. 1). During winter cooling, heat losses reach only as high as  $130 \text{ W m}^{-2}$  at  $30^\circ\text{N}$ ,  $140^\circ\text{W}$  (ESMW formation region), while heat losses in the CMW region exceed  $175 \text{ W m}^{-2}$  and near the Kuroshio in the western Pacific are greater than  $400 \text{ W m}^{-2}$  (da Silva et al. 1994). In this study, we will be concentrating on the formation mechanisms important in forming the deep late winter mixed layers associated with the CMW and ESMW formation regions.

The depth of the late winter mixed layer is dependent on a variety of factors including buoyancy fluxes, wind mixing, Ekman pumping, the background stratification, and advection. By using temperature and salinity (Levitus and Boyer 1994; Levitus et al. 1994) and heat flux (da Silva et al. 1994) climatologies to initialize and force a one-dimensional mixed layer model (Price et al. 1986), we hope to shed light on the interactions between some of these factors in forming the deep mixed layers observed in mode water formation regions.

The remainder of the paper is organized as follows: Section 2 provides a description of the mixed layer model. Section 3 discusses factors influencing mixed layer depth (MLD) in the ESMW region. Section 4 discusses factors influencing MLD in the CMW region. Section 5 discusses the negligible influence of wind mixing and freshwater fluxes on mixed layer depth. Section 6 provides discussion and conclusions.

## 2. Model

This study concentrates on the one-dimensional processes that contribute to the formation of deep mixed layers. In order to evaluate the relative importance of one-dimensional processes to mixed layer depth, a one-dimensional mixed layer model (Price et al. 1986) was used. The model calculates the density and wind-driven velocity profile in response to imposed atmospheric forcing (discussed below). Vertical mixing occurs in order to satisfy three stability criteria:

1. static stability:

$$\frac{\partial \rho}{\partial z} \geq 0,$$

2. mixed layer stability:

$$R_b \equiv \frac{g \Delta \rho h}{\rho_0 (\Delta V)^2} \geq 0.65,$$

3. shear flow stability:

$$R_g \equiv \frac{g \frac{\partial \rho}{\partial z}}{\rho_0 \left( \frac{\partial V}{\partial z} \right)^2} \geq 0.25,$$

where  $h$  is the mixed layer depth and  $\Delta(\ )$  is the difference between the mixed layer and the level just beneath (Price et al. 1986). Whenever any of these criteria is violated, the model mixes properties at neighboring (in the vertical) points on the model grid until the criteria are satisfied.

The model is run with a vertical resolution of  $\Delta z = 1.0 \text{ m}$  to a depth of  $400 \text{ m}$  (well below the mixed layer in the region of interest) and a time step of  $\Delta t = 864 \text{ s}$ . A control run was initialized with August temperature and salinity values from the *World Ocean Atlas 1994* monthly climatologies (Levitus and Boyer 1994; Levitus et al. 1994, hereafter WOA). The level data from the WOA were linearly interpolated to the vertical resolution of the model. Comparisons between the control run and test runs using various initial stratification patterns are discussed in sections 3 and 4. In addition, data from a July WOCE section at  $179^\circ\text{E}$  were used to initialize a model run in order to give insight into the effects of smoothing in the WOA data on our results. These results are discussed in section 4.

The Atlas of Surface Marine Data 1994 (da Silva et al. 1994, hereafter ASMD) monthly climatologies of surface heat fluxes (shortwave, longwave, sensible, and latent), evaporation minus precipitation ( $E - P$ ), and wind stresses were used as surface forcing for the mixed layer model. The monthly surface forcing from the ASMD was linearly interpolated to daily values in order to force the model. The model was run for 8 months, from August when the seasonal pycnocline is the

shallowest to March when the mixed layer is the deepest.

In order to evaluate the effectiveness of this one-dimensional model in reproducing the MLD in a system where three-dimensional processes are obviously important (more so in some regions than others), we ran a control run at each point over a large region of the North Pacific (20.5°–46.5°N, 149.5°E–130.5°W) for comparison with the “observed” MLD. At a 2° × 2° horizontal resolution, the model was run independently for each grid point (the results at each horizontal grid point do not effect the other grid points).

We have defined the MLD as the depth at which  $\sigma_\theta$  is 0.125 kg m<sup>-3</sup> different from the sea surface (following [Qiu and Huang 1995](#)). As the heat flux changes from positive (into the ocean) to negative (out of the ocean) in the autumn, the mixed layer begins to deepen ([Fig. 2](#)). The maximum heat flux out of the ocean averaged along 28.5°N occurs in December and does not become positive (into the ocean) until April. Averaged along 28.5°N, the MLD calculated by the model deepens more quickly than the MLD calculated from the WOA climatology resulting in a difference of roughly 90 m by the end of the run (March).

Both the March MLDs calculated from the WOA climatology ([Fig. 3a](#)) and those resulting from the control run ([Fig. 3b](#)) exhibit features thought to be associated with mode water formation regions. A maximum in March MLD (>220 m, [Fig. 3a](#)) south of the Kuroshio (30°–35°N, 140°–155°E) is associated with the western subtropical mode water ([Masuzawa 1969](#)). The STMW formation region is just outside of the model domain to the west. A local maximum associated with the ESMW formation region is apparent in both the MLD calculated from the WOA climatology (>120 m) and those calculated by the model (>160 m). This ESMW formation region is centered at approximately 30°N, 140°W in the eastern Pacific between Hawaii and the west coast of North America. In addition, a broad band of deep mixed layer (>240 m), associated with the central mode water ([Nakamura 1996; Suga et al. 1997](#)) is apparent in both calculations centered on approximately 40°N extending from about 150°E to the date line.

Although the spatial patterns are similar, the magnitudes are quite different, especially in the western Pacific. The model tends to overestimate MLDs and underestimate SST over most of the model domain relative to the WOA climatology. This overestimation is probably partially attributable to the effects of advection, especially in the western Pacific where the path of the Kuroshio, bringing warm water north, would be expected to have a large impact. An influx of warm surface water would tend to increase the stratification, which would decrease convective mixing.

In addition, due to the heavy spatial and temporal smoothing in the WOA climatology, maxima in MLD calculated from the climatology would tend to be underestimated. Spatial averaging tends to smooth out extremes in gradients resulting in overestimates of minima and underestimates of maxima. This results in an underestimate of MLD and an overestimate of stratification in the weakly stratified part of the water column at depth. In fact, mixed layer depths calculated from WOCE P16N CTD data taken along 152°W in the North Pacific in March ([McTaggart and Mangum 1995](#)) show maximum mixed layer depths reaching as deep as 140 m (around 30°–35°N), while those calculated from the WOA in the same region are less than 100 m. Thus, smoothing in the WOA and the resulting underestimate of MLDs may be partially responsible for the differences between MLDs calculated from the WOA and those calculated by the model. However, the effects of advection and other three-dimensional processes (neglected by the model) are probably much more important in explaining these differences.

An additional source of error comes from the fact that heat fluxes are notoriously difficult to determine. Heat flux climatologies such as the ASMD can be expected to have errors on the order of 20 W m<sup>-2</sup> (D. E. Harrison 1998, personal communication). So some of the difference between the model results and the WOA climatology may be due to errors in the heat flux forcing. To analyze the effects of possible errors in the heat flux climatology, we ran the model for two separate meridional sections with cooling reduced by 10 W m<sup>-2</sup>. Throughout this work, we will be concentrating on two meridional sections: 1) along 179.5°E, slicing through the MLD maximum associated with the CMW, and 2) along 140.5°W, associated with the ESMW. The differences between the model March MLD and SST and those calculated from the WOA average almost 46 m and 0.75°C, averaged along 179.5°E, with the model mixed layer deeper and colder than the WOA mixed layer. When the model is run with reduced cooling, the differences are reduced to about 24 m and 0.36°C, about half the original differences. Along 140.5°W, the differences were smaller than along 179.5°E: almost 33 m in MLD and 0.63°C in SST. The results of reducing the cooling reduced the difference in MLD to about 21 m and SST to 0.16°C. Thus errors in the heat flux climatology could certainly be a substantial part of the difference between modeled and observed MLD and SST.

The fact that the model gives deep mixed layers in the right places (as compared to the WOA) is encouraging. Since the model is initialized in late summer when the shallow stratification is the strongest, the one-dimensional processes, along with the initial stratification, included in the model must be at least partly responsible for the locations of the maxima in MLD. Our goal is to quantify the relative importance of wind mixing, buoyancy fluxes, and stratification on creating deep mixed layers in certain regions. Because of the simple one-dimensional nature of the model, it can be quite useful for analyzing the various effects of these processes and features on MLD, especially away from the western boundary where advection plays a very

important role.

### 3. Eastern subtropical mode water (140.5°W)

Using XBT data, HR98 identify the eastern subtropical mode water by a zone of minimum PV (defined in terms of temperature:  $PV = f\partial T/\partial z$ ) in the vertical centered at slightly more than 100-m depth. The PV minimum (calculated here in terms of density:  $PV = \rho^{-1} f\partial\sigma_\theta/\partial z$ ) is apparent in a zonal section of annually averaged WOA data at 29.5°N [Fig. 4a] after Nakamura (1996). The ESMW appears as a bullet of PV less than  $3.0 \times 10^{-10} \text{ m}^{-1} \text{ s}^{-1}$  located at 140°W at about 100-m depth. The associated  $\sigma_\theta$  (25.0–25.5  $\text{kg m}^{-3}$ ) (Fig. 4b) and temperature (17°–19°C) (Fig. 4c) ranges of this local PV minimum are consistent with those calculated by HR98 (24.0–25.4  $\text{kg m}^{-3}$ ; 16°–22°C). The salinity range of the ESMW is approximately 34.4–35.0 psu (Fig. 4d). The ESMW PV minimum lies just to the west of a salinity front associated with a tongue of fresh subpolar water extending southward along the coast of North America. To the west of this front, salinity has a destabilizing effect on the water column (saltier water overlying fresher water) while to the east of the front, salinity contributes to the stability of the water column. Farther to the east and deeper are stronger minima ( $PV < 2.0 \times 10^{-10} \text{ m}^{-1} \text{ s}^{-1}$ ) associated with the CMW (discussed in section 4) and STMW.

By superimposing contours of annual-mean acceleration potential on maps of PV on ESMW isopycnals, HR98 show that the mode water is circulated southward in the eastern part of the subtropical gyre away from the wintertime outcrop (the presumed formation region). Over the course of the year, the PV minimum shifts toward the southwest and weakens. The remains of the PV minimum water is found at 20°–25°N, 155°–130°W in early winter. (The PV minimum can be seen in the WOA data as far south as 24°N.) The PV minimum shifts roughly 7°–8° latitude in 8 months, giving a rough propagation speed of  $4 \text{ cm s}^{-1}$  (assuming purely meridional flow).

The formation region for ESMW is readily apparent by superimposing March SST contours and  $\sigma_\theta$  outcrops on a map of MLD (all derived from the WOA) (Fig. 3a). In a region centered at approximately 30°N, 140°W a locally deep mixed layer (MLD > 120 m) coincides with March surface temperatures between 16° and 20°C and lies just north of the  $\sigma_\theta = 25.0 \text{ kg m}^{-3}$  outcrop.

In the ESMW formation region (centered at 30°N, 140°W) winter cooling (Oct–Mar) averages only  $90 \text{ W m}^{-2}$  (da Silva et al. 1994). Because winter heat fluxes are small in the ESMW formation region (as compared to the CMW and STMW formation regions), the cause of the deep mixed layer has been unclear. HR98 suggest that the moderate winter heat loss observed in this region could induce convective mixed layer deepening if the water column was preconditioned toward lower stability.

Roden (1970, 1972) first identified a lateral minimum in the vertical stability in the North Pacific and termed it the “stability gap.” This region of reduced stability occurs in the subarctic–subtropical transition zone. North of the transition zone, stability is dictated by a strong permanent halocline. In the subtropical waters south of the transition zone, a strong thermocline results in high stability. In the transition zone in between, subpolar and subtropical water masses are both present, resulting in weaker stability. The reduced stability may allow vertical mixing to penetrate much deeper and could be one factor allowing the formation of mode waters in certain regions. Yuan and Talley (1996) calculate the horizontal minimum of vertical maximum buoyancy frequency from the Levitus (1982) winter data. They find that the stability gap occurs around 40°N in the western and central North Pacific. Another branch of the minimum is found near 30°N, coinciding with the ESMW formation region in the eastern Pacific.

The buoyancy frequency ( $N$ ) along 140.5°W calculated from WOA (Fig. 5) shows the stability gap quite clearly. Averaged over the winter (Jan–Mar) (Fig. 5a), the maximum (in the vertical) buoyancy frequency is greater than  $0.009 \text{ s}^{-1}$  except between 28° and 31°N—the stability gap—where  $N$  is between 0.008 and  $0.009 \text{ s}^{-1}$ . This maximum is associated with the main pycnocline and is observed at depth approximately 125 m at 46°N, deepening to 150–200-m depth at 20°N. This slope in pycnocline depth implies eastward geostrophic flow. The largest meridional gradient in pycnocline depth appears to occur in the region of the stability gap.

During the summer (Jul–Sep) (Fig. 5b), the vertical maximum of  $N$  is due to the seasonal pycnocline (formed by warming at the surface). The seasonal pycnocline also exhibits a stability gap. The vertical maximum  $N$  is greater than  $0.012 \text{ s}^{-1}$  north of 30°N. South of 30°N, the buoyancy frequency is between 0.010 and  $0.012 \text{ s}^{-1}$ . In October, at the end of the warming season, the weakest seasonal pycnocline in the North Pacific, as evidenced by the lowest values ( $N < 0.014$ ) of the vertical maximum in  $N$ , is seen in the eastern North Pacific at 20°–30°N, 150°–120°W [Fig. 6; after Yuan and Talley (1996)]. The ESMW formation region (and the summer stability gap shown in Fig. 5b) is in the northern part of this region. This summer stability gap is probably due to weak summer heating in this region.

The summer heating (averaged over Jun–Sep) (Fig. 1b) in this region is less than  $50 \text{ W m}^{-2}$  compared with values exceeding  $75 \text{ W m}^{-2}$  in other parts of the North Pacific. The region of low summer heating is a region of relatively low sea surface temperature (due to the tongue of cold subpolar water extending southward along the coast of North America) and high sea level pressure. Thus, dry subsiding air leads to high evaporation. At the same time, the cold sea surface temperature leads to an atmospheric temperature inversion that prevents the moist air from rising very far. This situation results in a thin layer of stratus clouds in this region during the summer (see Fig. 3 of Philander et al. 1996). Because stratus clouds are very reflective—they can reflect more than 30% of the incident solar radiation—they have a large effect on the incoming solar heat flux (Philander et al. 1996). The weak summer heating in this region is primarily due to the reduction of incoming solar radiation due to the stratus clouds. At  $30^\circ\text{N}$ ,  $140^\circ\text{W}$ , the net summer heating of about  $30 \text{ W m}^{-2}$  consists of roughly  $200 \text{ W m}^{-2}$  of incoming solar radiation offset by  $\sim 110 \text{ W m}^{-2}$  of outgoing latent heat flux and  $\sim 60 \text{ W m}^{-2}$  of outgoing sensible heat flux and longwave radiation. To the west of this region, the incoming solar radiation increases to about  $230 \text{ W m}^{-2}$ , while the other components of the net heat flux are relatively constant (da Silva et al. 1994).

To test whether the weak summer heating along  $140.5^\circ\text{W}$  would produce a weak seasonal pycnocline south of  $30^\circ\text{N}$ , the mixed layer model was initialized with March WOA temperature and salinity (the time of year when the water column is the least stratified). Then the model was run for five months forced by ASMD monthly summer heat flux,  $E - P$ , and wind stress. The August density field along  $140.5^\circ\text{W}$  derived from WOA (Fig. 7a) exhibits the weak stratification (low vertical density gradient and bowed up isopycnals) south of  $30^\circ\text{N}$ . The August density field resulting from the model run (Fig. 7b) exhibits a low vertical density gradient in the same region, demonstrating that the weak summer heating can in fact be responsible for the summer stability gap in this region.

In order to test the hypothesis that weak seasonal stratification during the summer is allowing deep mixed layers to form even though the heat fluxes are not very strong, we conducted three test runs of the mixed layer model in a meridional section along  $140.5^\circ\text{W}$  using different initial stratification fields. The control run (Figs. 8a,b), discussed in section 2, was initialized with August WOA temperature and salinity and forced with ASMD heat flux (Fig. 1),  $E - P$ , and wind stress. The first test run (run 1a) (Figs. 8c,d) was initialized with August WOA temperature and salinity at  $29.5^\circ\text{N}$  (the middle of the summer stability gap) over the entire meridional model domain (Fig. 8c). The second test run (run 2a) (Figs. 8e,f) was initialized with August WOA temperature and salinity at  $42.5^\circ\text{N}$  (a region with a strong seasonal pycnocline) over the entire meridional model domain (Fig. 8e). The third test run (run 3a) (Figs. 8g,h) was initialized with the same salinity profile as for run 1a (August  $29.5^\circ\text{N}$  salinity). The initial temperature profile, on the other hand, was constructed to simulate a strong seasonal pycnocline on top of the weak permanent pycnocline observed in the  $29.5^\circ\text{N}$  stratification. This temperature profile is the same as that for run 1a below 75-m depth. Shallower than 75-m depth,  $\Delta T/\Delta z$  calculated from the  $42.5^\circ\text{N}$  profile is used to construct a strong seasonal pycnocline. The forcing for the test runs was the same meridionally varying forcing as for the control run. The results of the four model runs along  $140.5^\circ\text{W}$  are summarized in Table 1.

The initial density field for the control run (Fig. 8a) exhibits strong seasonal stratification north of  $34^\circ\text{N}$ . Both temperature and salinity contribute to the strong gradient in this region. The vertical temperature gradient is much stronger north of  $34^\circ\text{N}$ . The vertical salinity gradient changes sign at about  $34^\circ\text{N}$ . North of  $34^\circ\text{N}$ , fresh water overlies salty water, contributing to strong stability. South of  $34^\circ\text{N}$ , salty water overlies fresh water, offsetting the stabilizing effects of an already weak temperature gradient. The control run combines this initial stratification and the applied forcing to result in a MLD greater than 150 m at  $28^\circ$ – $30^\circ\text{N}$  in the final (Mar) density field (Fig. 8b). The minimum MLD (68.2 m) occurs at  $46.5^\circ\text{N}$  and the maximum (185.5 m) occurs at  $28.5^\circ\text{N}$ .

A comparison between the stratification profiles used for the three test runs (Fig. 9) shows that the stratification profile used for run 1a ( $29.5^\circ\text{N}$ ) has a relatively weak seasonal pycnocline at 50 m (compared with the  $42.5^\circ\text{N}$  stratification) and a stratification minimum at 125 m associated with mode water formed the previous winter. The profile used to initialize run 2a ( $42.5^\circ\text{N}$ ) has a much stronger seasonal pycnocline at 30 m and does not exhibit the stability gap in the permanent pycnocline. The third profile (constructed for run 3a) is in some sense a combination of the two other profiles. It has a strong seasonal pycnocline derived from the  $42.5^\circ\text{N}$  profile and a weak permanent pycnocline copied from the  $29.5^\circ\text{N}$  profile.

Run 1a combines a weak initial stratification in both the seasonal and the permanent pycnoclines over the whole section with the same (meridionally varying) forcing as the control run. The initial density field for run 1a is the WOA  $29.5^\circ\text{N}$  stratification applied over the whole section. The vertical maximum in  $N$  in August at  $29.5^\circ\text{N}$  is  $0.0128 \text{ s}^{-1}$  at 50-m depth. This run results in a minimum MLD of 151.7 m at  $46.5^\circ\text{N}$  and a maximum MLD of 182.7 m at  $28.5^\circ\text{N}$ . The MLD is slightly shallower on the northern end of the model domain due to the slightly weaker heat flux there (Fig. 1c).

Run 2a combines the strong initial stratification at  $42.5^\circ\text{N}$  with the same forcing as the control run. At  $42.5^\circ\text{N}$ , in the region of stronger seasonal and permanent pycnoclines, the vertical maximum in August buoyancy frequency is  $0.0208 \text{ s}^{-1}$

at 30-m depth. When the August WOA temperature and salinity at 42.5°N is used to initialize the model (Fig. 8e), the same pattern in March MLD (minimum at 46.5°N and maximum at 28.5°N) results (Fig. 8f) as for run 1a, reflecting the pattern in the heat flux. The mixed layer is shallower with a minimum MLD of 67.7 m and a maximum MLD of 112.8 m.

In order to distinguish between the effects of the seasonal pycnocline and the permanent pycnocline on MLD, a third model run was executed. Run 3a was initialized with a stratification constructed in such a way as to keep the weak permanent pycnocline observed at 29.5°N but create a strong seasonal pycnocline in the upper 75 m of the water column. This run results in a maximum MLD of 158.8 m at 28.5°N. This MLD is almost 30 m shallower than that resulting from the control run illustrating that the weak seasonal pycnocline observed in the ESMW formation region contributes to the deep mixed layer there.

In these one-dimensional model runs, the MLD is a function of the heat flux forcing and the initial stratification. The following analysis is an attempt to quantify the relative effects of these two factors. In the simple case of a water column that is initially linearly stratified and subject to a constant surface cooling  $Q$  over a time period  $t$ , the depth  $h$  of the convective layer can be calculated from the heat and the mechanical energy budgets (see Cushman-Roisin 1994):

$$h = \frac{1}{N} \sqrt{\frac{6\alpha g Q t}{\rho_0 C_p}}, \quad (1)$$

where  $\alpha$  is the thermal expansion coefficient,  $g$  is gravitational acceleration, and  $N$  is the buoyancy frequency. In this simple case, the influences of stratification ( $N^2$ ) and heat flux ( $Q$ ) on MLD are inversely proportional to each other. Therefore, by keeping  $N^2$  or  $Q$  fixed and varying the other, the relative contributions of stratification and heat flux to the formation of deep mixed layers can be diagnosed.

Since we have eliminated the effect of stratification on the meridional variation of MLD in the test runs, any remaining meridional differences in MLD are solely due to the heat flux forcing. The heat flux at 28.5°N ( $Q_1$ ) averages 89 W m<sup>-2</sup> over the winter, while the heat flux at 46.5°N ( $Q_2$ ) averages 72 W m<sup>-2</sup> (Fig. 1c). Since the stratification in the two locations is meridionally unvarying for each test run, and assuming all other terms are constant, then

$$\frac{h_{28^\circ\text{N}}}{h_{46^\circ\text{N}}} = \sqrt{\frac{Q_{28^\circ\text{N}}}{Q_{46^\circ\text{N}}}}.$$


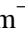
In addition, since the heat flux forcing is the same for all three test runs, any difference in MLD between the test runs is due solely to differences in stratification:

$$\frac{h_{1a}}{h_{2a}} = \frac{N_{2a}}{N_{1a}} \quad \text{OR} \quad \frac{h_{1a}}{h_{3a}} = \frac{N_{3a}}{N_{1a}}.$$


The square root of the ratio of  $Q_{28^\circ\text{N}}$  and  $Q_{46^\circ\text{N}}$  (using winter average  $Q$ ) is 1.1, while the ratio of  $N_{2a}$  and  $N_{1a}$  is 1.6 (using vertical maximum  $N$ ) or 1.5 (using  $N$  averaged over top 200 m) illustrating the difference between MLD at 28° and 46°N is due more to differing stratification at those two locations than to differing heat flux. The results are similar when comparing run 1a with run 3a.


The influence of the initial stratification on MLD can be further broken down into the influence of the shallow seasonal stratification relative to the influence of the deeper permanent stratification. The effect of the initial stratification on MLD at 28.5°N can be summarized by examining the three test runs. Because the heat flux forcing was the same for all three runs, the varying mixed layer depths are solely due to the initial stratification. The initial stratification for run 1a (weak seasonal pycnocline and weak permanent pycnocline) results in a MLD of 182.7 m. The initial stratification for run 2a (strong seasonal pycnocline and strong permanent pycnocline) results in a MLD of 112.8 m. Run 3a, with a strong seasonal pycnocline and a weak permanent pycnocline, results in a MLD of 158.8 m. The results of these model simulations suggest that, in the ESMW region, both the weak permanent stratification and the weak summer stratification (probably due to weak summer heating) have an effect (of approximately the same magnitude) on the formation of locally deep mixed layers and thus on mode water formation.


#### 4. Central mode water (179.5°E)





[Nakamura \(1996\)](#) identifies the central mode water as a layer of low PV water at the densest levels (approximately  $\sigma_\theta = 26.2 \text{ kg m}^{-3}$ ) of the ventilated pycnocline. The  $\sigma_\theta = 26.0\text{--}26.5 \text{ kg m}^{-3}$  isopycnals outcrop in the winter near the subarctic–subtropical transition zone, the northernmost outcropping area of the subtropical main thermocline. As mentioned in [section 3](#), potential vorticity calculated from annually averaged WOA data along  $29.5^\circ\text{N}$  shows two regions with a minimum of PV less than  $2.0 \times 10^{-10} \text{ m}^{-1} \text{ s}^{-1}$  ([Fig. 4a](#) ). The westernmost, shallow PV minimum (250-m depth,  $140^\circ\text{E}\text{--}180^\circ$ ) has a density of approximately  $\sigma_\theta = 25.5 \text{ kg m}^{-3}$  ([Fig. 4b](#) ) and corresponds to the STMW. The section of the PV minimum that lies between  $\sigma_\theta = 26.0\text{--}26.5 \text{ kg m}^{-3}$  corresponds to the CMW. Just below this layer (heavier than  $\sigma_\theta = 26.5 \text{ kg m}^{-3}$ ) is the North Pacific Intermediate Water, which is not ventilated in the subtropical gyre ([Nakamura 1996](#)). [Warner et al. \(1996\)](#) attribute a CFC maximum with an associated oxygen maximum at densities near  $\sigma_\theta = 25.9 \text{ kg m}^{-3}$  ( $11^\circ\text{--}14^\circ\text{C}$ ) at  $24^\circ\text{N}$  between  $160^\circ$  and  $140^\circ\text{W}$  to the CMW.


The entire CMW thermostad appears to lie in a zone of eastward flow, the North Pacific Current ([Suga et al. 1997](#)). Eastward flow with a slight southward component is dominant over the formation region. The typical eastward geostrophic speed of about  $5 \text{ cm s}^{-1}$  relative to 2000 dbar [derived from [Levitus \(1982\)](#) climatology] is consistent with the fact that the annual mean center of the mode water distribution is roughly  $10^\circ$  of longitude to the east of the wintertime formation area ([Suga et al. 1997](#)).



[Nakamura \(1996\)](#) finds a region with SST equal to CMW temperatures ( $8.5^\circ\text{--}11.5^\circ\text{C}$ ) coinciding with winter mixed layer depth (defined by  $\Delta T \equiv 1^\circ\text{C}$ ) greater than 200 m east of approximately  $170^\circ\text{E}$  and north of roughly  $39^\circ\text{N}$ . The region is separated from the STMW region by an area with moderate winter mixed layer depth (150–200 m) ([Nakamura 1996](#); [Suga et al. 1997](#)). The  $\Delta\sigma_\theta \equiv 0.125 \text{ kg m}^{-3}$  definition for MLD results in a band of deep winter mixed layer (MLD > 220 m) centered at about  $41^\circ\text{N}$  extending from approximately  $150^\circ\text{E}$  to the date line. The easternmost part of this zone of deep March mixed layer (around the date line) has a March SST range ( $8^\circ\text{--}12^\circ\text{C}$ ) consistent with those estimated by [Nakamura \(1996\)](#) and [Suga et al. \(1997\)](#). In addition, this region lies just north of the March outcrop of the  $\sigma_\theta = 26.3 \text{ kg m}^{-3}$  surface ([Fig. 3a](#) ).

This region has much higher winter heat losses than the ESMW region but still not as high as the STMW region ([Fig. 1a](#) ). As noted in [section 3](#), the stability gap is observed at around  $40^\circ\text{N}$  in the western and central North Pacific ([Yuan and Talley 1996](#)). So, once again, we can try to determine the relative importance of the heat fluxes and the background stratification to the formation of deep winter mixed layers.

The average winter (Jan–Mar) buoyancy frequency along  $179.5^\circ\text{E}$  calculated from WOA ([Fig. 10a](#) ) exhibits a stability gap between  $32^\circ$  and  $44^\circ\text{N}$ . The vertical maximum in stability is greater than  $0.005 \text{ s}^{-1}$  except between these latitudes where  $N$  is between  $0.003$  and  $0.005 \text{ s}^{-1}$  (about half the vertical maximum in winter buoyancy frequency in the ESMW formation region). The depth of the pycnocline (depth where the maximum  $N$  occurs) is between 100 and 150 m except in the region of the stability gap where it is much deeper. As in the ESMW region, the largest meridional gradients in the depth of the pycnocline (consistent with the eastward geostrophic flow of the North Pacific Current) occur in the region of the stability gap.

Averaged over the summer (Jul–Sep), maximum stratification in the vertical at  $179.5^\circ\text{E}$  ([Fig. 10b](#) ) is quite strong ( $0.015 \text{ s}^{-1} < N < 0.022 \text{ s}^{-1}$ ) over the whole section as compared to the ESMW region ( $140.5^\circ\text{W}$ ) where maximum values of  $N$  are between  $0.010 \text{ s}^{-1}$  and  $0.019 \text{ s}^{-1}$  ([Fig. 5b](#) , also see [Fig. 6](#) ). In addition, the two mode water formation regions (with maximum summer stratification in the top 400 m  $< 0.020 \text{ s}^{-1}$ ) appear to be separated by a band with maximum summer stratification greater than  $0.020 \text{ s}^{-1}$  that stretches across the North Pacific from approximately  $22^\circ\text{N}$ ,  $135^\circ\text{E}$  to  $45^\circ\text{N}$ ,  $150^\circ\text{W}$  ([Fig. 6](#) ).

In the  $179.5^\circ\text{E}$  section, the stability is maximum in the region between  $30^\circ$  and  $38^\circ\text{N}$ . Although there is an obvious stability gap in the CMW formation region in the winter ([Fig. 10a](#) ) , no stability gap is evident in the seasonal pycnocline during the summer. However, at depth ( $\sim 200 \text{ m}$ ), the summer stratification is weakest ( $< 0.004 \text{ s}^{-1}$ ) north of  $38^\circ\text{N}$  (in the region of CMW formation).

The buoyancy frequency calculated using data from the WOCE P14N meridional section at  $179^\circ\text{E}$  in July 1993 ([Rodén and Fredericks 1995a,b](#)) ([Fig. 11](#) ) is shown as a comparison to that calculated from WOA ([Fig. 10b](#) ). The heavy smoothing of the WOA dataset is apparent in the comparison. This smoothing averages out extremes in water property gradients. The maximum buoyancy frequency in the WOCE section is greater than  $0.037 \text{ s}^{-1}$ , while the maximum buoyancy



frequency in the WOA data in the same region is  $0.023 \text{ s}^{-1}$ . However, the overall structure of the buoyancy frequency field is much the same. The WOCE data exhibits the strong ( $>0.02 \text{ s}^{-1}$ ) seasonal pycnocline at about 50-m depth. In addition, the weak deeper stratification ( $<0.004 \text{ s}^{-1}$ ) north of  $38^\circ\text{N}$  is also apparent in both datasets.

Once again, two test runs (plus the previously discussed control run) of the mixed layer model were used to test the dependence of deep mixed layer formation at  $179.5^\circ\text{E}$  on initial summer stratification. The first test run (run 1b) (Figs. 12c,d) was initialized with August WOA temperature and salinity at  $41.5^\circ\text{N}$  (the region of the winter stability gap and the deepest mixed layers in the control run). The second test run (run 2b) (Figs. 12e,f) was initialized with August WOA temperature and salinity at  $26.5^\circ\text{N}$  (a region of stronger stability and shallower control run mixed layer depth). The two test runs were initialized with meridionally invariant stratification (temperature and salinity) but forced with the same meridionally varying heat flux,  $E - P$ , and wind stress forcing as the control run. The results of the control run and the two test runs are summarized in Table 2.

The control run at  $179.5^\circ\text{E}$  (Figs. 12a,b) was initialized with WOA August temperature and salinity and forced with monthly varying heat fluxes, wind stress, and  $E - P$ . The initial density field (Fig. 10a) exhibits a strong seasonal pycnocline at roughly 50-m depth throughout most of the meridional section. At the southern end of the section, the seasonal pycnocline is somewhat weaker and slightly deeper. The heat flux forcing consists of two local maxima in cooling: at  $38.5^\circ\text{N}$  cooling (averaged over Oct through Mar) is greater than  $155 \text{ W m}^{-2}$  and at  $26.5^\circ\text{N}$  cooling is greater than  $119 \text{ W m}^{-2}$  (Fig. 1c). The resulting March MLD is maximum ( $>300 \text{ m}$ ) at  $38.5^\circ\text{N}$  (Fig. 12b) where the cooling is the strongest, and minimum (62.7 m) at  $46.5^\circ\text{N}$  where the cooling is weakest (Fig. 1c). No local maximum in March MLD is apparent in the region of the smaller of the two local heat flux maxima due to the fact that the deep (100–250 m) stratification is stronger there.

In order to test the effects of the smoothing in the WOA data on the model simulations, the July 1993 WOCE section at  $179^\circ\text{E}$  was used to initialize a model run (Fig. 13). This model run used the same forcing as the control run (except at  $1^\circ$  resolution as opposed to  $2^\circ$  for the control run). The resulting March MLD reaches as deep as 400 m between  $37.5^\circ$  and  $41.5^\circ\text{N}$  (Fig. 13b). The minimum MLD (88 m) occurs at  $46.5^\circ\text{N}$ . These results are encouraging in that the MLD pattern looks similar to the pattern of MLD resulting from the control run. The main difference is that mixed layer depths resulting from the WOCE section run are deeper than those resulting from the control run. As discussed previously, smoothing in the WOA data results in underestimates of maxima and overestimates of minima. At  $179^\circ\text{E}$ , the minima in deep stratification are overestimated in the WOA data (minimum  $N$  in WOA data is  $0.003 \text{ s}^{-1}$ ; minimum  $N$  in WOCE section is  $0.0004 \text{ s}^{-1}$ ). Thus, once the mixing penetrates through the seasonal pycnocline, the mixing encounters more resistance in the control run than in the WOCE run. This results in a deeper March mixed layer for the WOCE initialized run. Based on this comparison, smoothing of the WOA dataset may result in an underestimate of the contribution of stratification (relative to heat flux effects) on MLD in our analysis.

The initial stratification for run 1b (Fig. 12c) consists of a maximum buoyancy frequency of  $0.024 \text{ s}^{-1}$  at depth 25 m and buoyancy frequencies less than  $0.0045 \text{ s}^{-1}$  between 150 and 400 m. This run results in a MLD with two local maxima (Fig. 12d): 320 m at  $38.5^\circ\text{N}$  and 300 m at  $26.5^\circ\text{N}$  reflecting the two maxima in the heat flux forcing. The minimum MLD of 69 m occurs at  $46.5^\circ\text{N}$  where the heat fluxes are not strong enough to completely erode through the summer stratification.

The initial stratification for run 2b (Fig. 12e) consists of a maximum buoyancy frequency of  $0.024 \text{ s}^{-1}$  at depth 40 m and buoyancy frequencies between  $0.005$  and  $0.007 \text{ s}^{-1}$  between 150 and 400 m. The MLD resulting from this model run also shows the double maxima but at a much shallower depth: 177 m at  $38.5^\circ\text{N}$  and 137 m at  $26.5^\circ\text{N}$ . That the initial maximum stratification is similar between this run and run 1b but the MLD is shallower illustrates that the shallow stratification is not the factor allowing deep mixed layers in this region. The minimum MLD (71.3 m) occurs at  $46.5^\circ\text{N}$  and is not much different than for either the control run or run 1b.

At  $179.5^\circ\text{E}$ , the winter cooling is much stronger than at  $140.5^\circ\text{W}$ . The stronger cooling erodes the seasonal pycnocline except at the northernmost part of the section where the cooling is almost as weak as at  $140.5^\circ\text{W}$ . Once the seasonal pycnocline has been fully eroded, the deeper stratification comes into play. The interplay between the weak stratification below 150 m and the maximum in cooling at  $38^\circ\text{N}$  allows for deep mixed layers there.

In section 3, we compared the relative contribution of stratification and heat fluxes to MLD by assuming a relationship between the two effects. In the ESMW formation region, the effect of stratification on MLD is larger than the effect of heat flux. In contrast, at  $179.5^\circ\text{E}$  in the CMW formation region, the shift in mean MLD between run 1b and run 2b (attributable to the different stratification fields between the two runs) is 118.5 m, while the average range of MLD over the meridional section (attributable to heat flux effects) was 178.4 m. Thus, in the CMW formation region, heat fluxes have a stronger impact on MLD than the initial background stratification.

## 5. Wind mixing and $E - P$

The effect of wind mixing on deepening the mixed layer and the contribution of evaporation and precipitation to buoyancy fluxes have largely been ignored in discussions of mode water formation. However, since both the CMW and the ESMW formation regions occur within the transition zone between the subtropical and the subpolar gyres where there are high meridional gradients in surface salinity,  $E - P$  sign changes, and fairly high wind speeds, it is worthwhile to test the influence of these two processes on mixed layer depth.

Once again, model runs were conducted along two meridional sections:  $179.5^{\circ}\text{E}$  and  $140.5^{\circ}\text{W}$ . The model was run with heat flux forcing only (no  $E - P$  forcing or wind mixing) and compared to the control run discussed above. The  $E - P$  and wind mixing had essentially no impact on MLD. In the  $140.5^{\circ}\text{W}$  section, the control run produced a maximum in MLD at  $28.5^{\circ}\text{N}$  of 185.5 m, while the run with zero  $E - P$  and wind mixing produced a maximum at the same place of 182.2 m, a difference of less than 2%. At  $179.5^{\circ}\text{E}$  where the heat fluxes are higher, the maximum MLD is decreased by less than 0.5% when the model is run without wind or  $E - P$  forcing. In addition, the model was run with heat flux forcing and wind mixing but no  $E - P$  forcing in order to make sure that the effects of  $E - P$  and wind mixing were not offsetting each other. These runs also resulted in essentially no difference from the control run. Thus, based on the results of these model simulations, wind mixing and  $E - P$  forcing have a negligible effect on MLD in the CMW and ESMW formation regions compared to heat flux forcing.

## 6. Summary and discussion

The effects of one-dimensional processes on the formation of deep mixed layers in the central mode water and eastern subtropical mode water formation regions of the North Pacific have been analyzed using a mixed layer model ([Price et al. 1986](#)). By running the model with various combinations of initial (Aug) background stratification and forcing fields (heat flux,  $E - P$ , and wind mixing) and comparing the resultant March mixed layer depths, the relative importance of these effects on creating deep mixed layers was diagnosed.

Model results suggest that the contributions of evaporation minus precipitation and wind mixing to mixed layer deepening in both the CMW and the ESMW formation regions are negligible. Thus, the primary focus of this work is on describing the influence of the structure of the initial background stratification. Due to the fact that heat fluxes are weaker in these regions than in the classical subtropical mode water formation region in the western North Pacific, it was hypothesized that preconditioning of the water column to reduce stratification is necessary in order for the weaker cooling to form deep mixed layers.

In the ESMW formation region at  $140.5^{\circ}\text{N}$ , model results confirm that the initial stratification is important in determining where deep mixed layers will form. The summer heat flux has largely been ignored in analysis of mode water formation. However, due to stratus cloud cover the summer heating is quite weak in this region, resulting in a weak (or even nonexistent) seasonal pycnocline at the end of the summer at about  $30^{\circ}\text{N}$ . This lack of shallow seasonal stratification is partially responsible for allowing the mixed layer to become deep even though the wintertime cooling is much weaker here than in other regions of deep mixed layers. Weak deeper stratification associated with mode water formed in previous years also plays a role.

Because the shallow stratification is directly related to surface forcing, it is probably fairly variable. [Ronca and Battisti \(1997\)](#) calculate a mean summertime (Jun–Oct) net heat flux of  $47 \text{ W m}^{-2}$  with a summertime variance of  $650 (\text{W m}^{-2})^2$  from Ocean Weather Station N data at  $30^{\circ}\text{N}$ ,  $140^{\circ}\text{W}$ . If the summertime surface heating is variable on an interannual timescale, then the formation of ESMW might be expected to be variable as well. However, ESMW formation is also dependent on the weak stratification deeper in the water column that is a remnant of mode water from previous years. The influence of this deeper stratification may damp the effects of variability in the surface forcing. Thus, interannual variability of ESMW properties and formation rates is likely to be complicated.

HR98 note a possible biannual variation in the inventory of ESMW with years of strong mode water formation followed by years of weak mode water formation. Attempts at comparing summer averaged heat flux anomalies from the ASMD to the areal inventory of ESMW calculated by HR98 were inconclusive. However, variability of mode water formation mechanisms could result in variability in the area over which mode water forms (areal inventory), variability in the depth to which it forms (magnitude of the PV minimum), variability in the temperature of mode water formed, or more likely a combination of the three. It would probably be more appropriate to compare the strength of heat flux anomalies with the strength of the PV minimum.

Mixing between currently forming mode water and mode water formed in previous years may effect mode water properties. [Namias and Born \(1970, 1974\)](#) first noted a tendency for midlatitude SST anomalies to recur in succeeding winters without persisting through the intervening summer. They speculated that temperature anomalies in the deep winter

mixed layer could remain intact in the seasonal thermocline during the summer, insulated from surface processes by the shallow summer stratification. These anomalies could then affect the temperature of the succeeding winter's deep mixed layer. In fact, [Alexander and Deser \(1995\)](#), using a one-dimensional mixed layer model similar to the one used in this study, find that vertical mixing processes allow ocean temperature anomalies created over a deep winter mixed layer to be preserved below the surface in summer to reappear in the mixed layer in the following autumn. Using a three-dimensional model of the North Pacific, [Miller et al. \(1994\)](#) find that this reemergence mechanism is weak over most of the central Pacific (in the region of the California Current and the Kuroshio Extension) but does occur in the vicinity of the ESMW formation region.

In the CMW formation region, in contrast to the ESMW formation region, wintertime cooling is strong enough to erode through the shallow seasonal pycnocline. In the region of deepest mixed layers in the CMW region, the deeper stratification (150–400 m) is quite weak. Once the seasonal pycnocline has been fully eroded, the deeper stratification becomes important in allowing the mixing to penetrate further.

Of course this analysis, using the one-dimensional mixed layer model, has ignored any advective effects. These effects are likely to be quite important in some locations. In fact, a local maximum in WOA March mixed layer depth ([Fig. 3a](#)) of over 290 m occurs around 160°E, approximately 19° to the west of the maximum MLD we have associated with the CMW formation region. [Suga et al. \(1997\)](#) estimate an eastward geostrophic speed of approximately  $5 \text{ cm s}^{-1}$  ( $\sim 19^\circ \text{ long. yr}^{-1}$ ) relative to 2000 dbar over this region. If the weak subsurface stratification formed by the deep March mixed layer at 160°E advected approximately 19° of longitude in a year, it could be responsible for the weak deep stratification that contributes to the formation of CMW. Attempts to follow up on this hypothesis by analyzing WOA data were unsuccessful. Some factors that may be responsible for our lack of success in tracking the advection of subsurface stratification include effects of the meridional component of currents or of vertical shear in the water column, which were not taken into account in the analysis. In addition, the effects of temporal and spatial smoothing on the WOA data may have had some influence.

The influence of horizontal advection on ESMW formation is not likely to be as important as to the CMW formation for a couple of reasons: 1) the shallow seasonal stratification is important to ESMW formation and this weak stratification is more recently and locally formed than the deeper stratification important to CMW formation and 2) the ESMW formation region is in the broad region of weaker southward flowing currents.

In addition to horizontal advection, Ekman pumping may also be important to deep mixed layer formation. In fact, [Talley \(1988\)](#) notes that the lateral minimum in potential vorticity associated with the ESMW lies under a region of maximum Ekman downwelling [calculated from [Han and Lee's \(1981\)](#) wind stress analysis]. On the other hand, [Nakamura \(1996\)](#) points out that the CMW formation region lies in the subtropical gyre south of the zero Sverdrup function but in the upwelling region north of the zero in Ekman pumping. He concludes that Ekman pumping cannot be important in the subduction of CMW.

These conclusions are supported by [Huang and Qiu \(1994\)](#). They calculate subduction rates from [Levitus \(1982\)](#) climatology and [Hellerman and Rosenstein \(1983\)](#) wind stress data. Their calculations show a local maximum in subduction rate greater than  $25 \text{ m yr}^{-1}$  around 42°N, 160°E that may be associated with CMW formation. This maximum is almost completely due to lateral induction (where water parcels move laterally across the sloping base of the mixed layer). In addition, a double maximum in subduction rate greater than  $50 \text{ m yr}^{-1}$  that may be associated with the ESMW is evident in the region 20°–30°N, 140°–120°W. This maximum is due to both lateral induction and vertical pumping in approximately equal parts.

Formation of mode waters is obviously a complicated process depending on the interplay of various oceanic and atmospheric factors. We have only focused on the one-dimensional processes that lead to deep mixed layers, an important feature in mode water formation. The formation and circulation of mode water is much more complex than this analysis would suggest.

[Yasuda and Hanawa \(1997\)](#) study decadal changes in the STMW and the CMW by averaging together (seasonally) all data from the decade 1966–75 and comparing it to data averaged over 1976–85. In the mid-1970s, a well-documented transition occurred in the North Pacific ([Douglas et al. 1982](#); [Nitta and Yamada 1989](#); [Graham 1994](#); [Deser et al. 1996](#)). This transition resulted in a decrease in SST in the central North Pacific that lasted into the 1980s. The transition has been shown to have a connection with variations in atmospheric circulation characterized by the Pacific–North American (PNA) pattern ([Trenberth 1990](#); [Wallace et al. 1990](#); [Trenberth and Hurrell 1994](#)). [Yasuda and Hanawa \(1997\)](#) find that the CMW was colder and more widely distributed during 1976–85 compared to the previous decade. They attribute this cooling to increased Ekman heat divergence in the CMW formation region caused by intensification of the westerlies (associated with an enhanced Aleutian low).

[Zhang and Levitus \(1997\)](#) provide observational evidence of decadal variability in the thermal structure of the subsurface ocean. They present evidence that the temperature anomaly patterns rotate anticyclonically around the subtropical gyre with

a characteristic timescale of approximately 20 yr. Maxima in the spatial pattern of this variability shows good correspondence with the formation regions of the CMW and the ESMW, suggesting that variability in mode water formation in these two regions may be related to decadal variability in the North Pacific.

Recent studies have suggested that water parcels subducted in the subtropical North Pacific may provide a link between the midlatitude and the tropical ocean. This link may influence subtropical and tropical variability on decadal timescales (Gu and Philander 1997; Zhang et al. 1998). It has been hypothesized that subducted thermal anomalies can propagate equatorward in the thermocline (Gu and Philander 1996; Schneider et al. 1999), eventually upwelling and affecting sea surface temperatures in the Tropics and perhaps the frequency or magnitude of El Niño events. The atmosphere could then respond to the anomalous SST and, through teleconnections (Bjerknes 1966; Alexander 1992; Philander 1990), affect the surface ocean in the subtropics thus influencing decadal variability. In fact, Schneider et al. (1999), using a dataset of BT, XBT, and CTD stations compiled by White (1995), succeed in tracking anomalies in the depth of the 12°–18°C isothermal layer from the central North Pacific to approximately 20°N.

Because the western subtropical mode water is formed in, and primarily confined to, the recirculation region of the western subtropical gyre, it is not likely to be a participant in the subtropical–tropical exchange. General circulation models have been used to deduce the pathways taken by subducted water parcels (Gu and Philander 1997). Results suggest that the water masses formed farther to the east, such as the ESMW, are the most likely to have an influence on the Tropics. Thus, an understanding of the circulation and variability of these mode waters is important to our understanding of decadal variability.

### Acknowledgments

We are grateful to Susan Hautala, Sabine Mecking, and Kathryn Kelly for many helpful discussions. Comments from two anonymous reviewers helped to improve the original manuscript. This work was supported by the National Aeronautics and Space Administration through an Earth System Science Graduate Fellowship (Ladd) and Contract 960888 with the Jet Propulsion Laboratory (TOPEX/Poseidon Science Working Team) (Thompson).

---

## REFERENCES

- Alexander, M. A., 1992: Midlatitude atmosphere ocean interaction during El Niño. Part I: The North Pacific Ocean. *J. Climate*, **5**, 944–958. [Find this article online](#)
- , and C. Deser, 1995: A mechanism for the recurrence of wintertime midlatitude SST anomalies. *J. Phys. Oceanogr.*, **25**, 122–137. [Find this article online](#)
- Bjerknes, J., 1966: A possible response to the atmospheric Hadley circulation to equatorial anomalies of temperature. *Tellus*, **18**, 820–829.
- Cushman-Roisin, B., 1987: On the role of heat flux in the Gulf Stream–Sargasso Sea subtropical gyre system. *J. Phys. Oceanogr.*, **17**, 2189–2202. [Find this article online](#)
- , 1994: *Introduction to Geophysical Fluid Dynamics*. Prentice-Hall, 320 pp.
- da Silva, A. M., C. C. Young, and S. Levitus, 1994: *Atlas of Surface Marine Data 1994*. Vol. 1: *Algorithms and Procedures*. NOAA Atlas NESDIS 6, 51 pp.
- Deser, C., M. A. Alexander, and M. S. Timlin, 1996: Upper-ocean thermal variations in the North Pacific during 1970–1991. *J. Climate*, **9**, 1840–1855. [Find this article online](#)
- Douglas, A. V., D. R. Cayan, and J. Namias, 1982: Large-scale changes in North Pacific and North American weather patterns in recent decades. *Mon. Wea. Rev.*, **110**, 1851–1862. [Find this article online](#)
- Graham, N. E., 1994: Decadal-scale climate variability in the tropical and North Pacific during the 1970s and 1980s: Observations and model results. *Climate Dyn.*, **6**, 135–162.
- Gu, D., and S. G. H. Philander, 1997: Interdecadal climate fluctuations that depend on exchanged between the tropics and extratropics. *Science*, **275**, 805–807.
- Han, Y. J., and S. W. Lee, 1981: A new analysis of monthly mean wind stress over the global ocean. Climatic Research Institute Rep. No. 26, Oregon State University, 148 pp.

Hautala, S. L., and D. H. Roemmich, 1998: Subtropical mode water in the Northeast Pacific Basin. *J. Geophys. Res.*, **103**, 13 055–13 066..

Hellerman, S., and M. Rosenstein, 1983: Normal monthly wind stress over the world ocean with error estimates. *J. Phys. Oceanogr.*, **13**, 1093–1104.. [Find this article online](#)

Huang, R. X., and B. Qiu, 1994: Three-dimensional structure of the wind driven circulation in the subtropical North Pacific. *J. Phys. Oceanogr.*, **24**, 1608–1622.. [Find this article online](#)

Levitus, S., 1982: *Climatological Atlas of the World Ocean*. NOAA Prof. Paper No. 13, U.S. Govt. Printing Office, Washington, DC, 173 pp..

— , and T. P. Boyer, 1994: *World Ocean Atlas 1994*. Vol. 4: *Temperature*. NOAA Atlas NESDIS 4, 117 pp..

— , R. Burgett, and T. P. Boyer, 1994: *World Ocean Atlas 1994*. Vol. 3: *Salinity*. NOAA Atlas NESDIS 3, 99 pp..

Marshall, J. C., A. J. G. Nurser, and R. G. Williams, 1993: Inferring the subduction rate and period over the North Atlantic. *J. Phys. Oceanogr.*, **23**, 1315–1329.. [Find this article online](#)

Masuzawa, J., 1969: Subtropical mode water. *Deep-Sea Res.*, **16**, 463–472..

— , 1972: Water characteristics of the North Pacific Central Region. *Kuroshio—Its Physical Aspects*, H. Stommel and K. Yoshida, Eds., University of Tokyo Press, 235–352..

McTaggart, K. E., and L. J. Mangum, 1995: CTD measurements collected on a climate and global change cruise (WOCE section P16N) along 152°W during February–April, 1991. NOAA Data Report ERL PMEL-53, 227 pp..

Miller, A. J., D. R. Cayan, and J. M. Oberhuber, 1994: On the re-emergence of midlatitude SST anomalies. *Proc. 18th Annual Climate Diagnostic Workshop*, Boulder, CO, NOAA, 149–152..

Nakamura, H., 1996: A pycnostad on the bottom of the ventilated portion in the central subtropical North Pacific: Its distribution and formation. *J. Oceanogr.*, **52**, 171–188..

Namias, J., and R. M. Born, 1970: Temporal coherence in North Pacific sea surface temperatures. *J. Geophys. Res.*, **79**, 797–798..

— , and — , 1974: Further studies of temporal coherence in North Pacific sea-surface temperature patterns. *J. Geophys. Res.*, **75**, 5952–5955..

Nitta, T., and S. Yamada, 1989: Recent warming of tropical sea surface temperature and its relationship to the Northern Hemisphere circulation. *J. Meteor. Soc. Japan*, **67**, 375–383..

Philander, S. G. H., 1990: *El Niño, La Niña and the Southern Oscillation*. Academic Press, 293 pp..

— , D. Gu, D. Halpern, G. Lambert, N.-C. Lau, T. Li, and R. C. Pacanowski, 1996: Why the ITCZ is mostly north of the equator. *J. Climate*, **9**, 2958–2972.. [Find this article online](#)

Price, J. F., R. A. Weller, and R. Pinkel, 1986: Diurnal cycling: Observations and models of the upper ocean response to diurnal heating, cooling and wind mixing. *J. Geophys. Res.*, **91**, 8411–8427..

Qiu, B., and R. X. Huang, 1995: Ventilation of the North Atlantic and North Pacific: Subduction versus obduction. *J. Phys. Oceanogr.*, **25**, 2374–2390.. [Find this article online](#)

Roden, G. I., 1970: Aspects of the mid-Pacific transition zone. *J. Geophys. Res.*, **75**, 1097–1109..

— , 1972: Temperature and salinity fronts at the boundary of the subarctic-subtropical transition zone in the western Pacific. *J. Geophys. Res.*, **77**, 7175–7187..

— , and W. J. Fredericks, 1995a: World Ocean Circulation Experiment. Pacific Ocean, WOCE P14N, R/V Thomas G. Thompson Cruise 5 July–1 September 1993. CTD Data Report Part 1: Listings. University of Washington School of Oceanography Contribution 2111, 388 pp..

— , and — , 1995b: World Ocean Circulation Experiment. Pacific Ocean, WOCE P14N, R/V Thomas G. Thompson Cruise 5 July–1 September 1993. CTD Data Report Part 2: Profiles. University of Washington School of Oceanography Contribution 2111, 586 pp..

Roemmich, D., and B. Cornuelle, 1992: The subtropical mode waters of the South Pacific Ocean. *J. Phys. Oceanogr.*, **22**, 1178–1187.. [Find this article online](#)

Ronca, R. E., and D. S. Battisti, 1997: Anomalous sea surface temperatures and local air–sea energy exchange on intraannual timescales in the northeastern subtropical Pacific. *J. Climate*, **10**, 102–117.. [Find this article online](#)

Schneider, N., A. J. Miller, M. A. Alexander, and C. Deser, 1999: Subduction of decadal North Pacific temperature anomalies: Observations and dynamics. *J. Phys. Oceanogr.*, **29**, 1056–1070.. [Find this article online](#)

Siedler, G., A. Kuhl, and W. Zenk, 1987: The Madeira mode water. *J. Phys. Oceanogr.*, **17**, 1561–1570.. [Find this article online](#)

Stommel, H., 1979: Determination of watermass properties of water pumped down from the Ekman layer to the geostrophic flow below. *Proc. Natl. Acad. Sci. U.S.A.*, **76**, 3051–3055..

Suga, T., Y. Takei, and K. Hanawa, 1997: Thermostat distribution in the North Pacific subtropical gyre: the central mode water and the subtropical mode water. *J. Phys. Oceanogr.*, **27**, 140–152.. [Find this article online](#)

Talley, L. D., 1988: Potential vorticity distribution in the North Pacific. *J. Phys. Oceanogr.*, **18**, 89–106.. [Find this article online](#)

Trenberth, K. E., 1990: Recent observed interdecadal climate changes in the Northern Hemisphere. *Bull. Amer. Meteor. Soc.*, **71**, 988–993.. [Find this article online](#)

—, and J. W. Hurrell, 1994: Decadal atmosphere–ocean variations in the Pacific. *Climate Dyn.*, **9**, 303–319..

Wallace, J. M., C. Smith, and Q. Jiang, 1990: Spatial patterns of atmosphere–ocean interaction in the northern winter. *J. Climate*, **3**, 990–998.. [Find this article online](#)

Warner, M. J., J. L. Bullister, D. P. Wisegarver, R. H. Gammon, and R. F. Weiss, 1996: Basin-wide distributions of chlorofluorocarbons CFC-11 and CFC-12 in the North Pacific: 1985–1989. *J. Geophys. Res.*, **101**, 20 525–20 542..

White, W. B., 1995: Design of a global observing system for gyre-scale upper ocean temperature variability. *Progress in Oceanography*, Vol. 36, Pergamon, 169–217..

Woods, J. D., 1985: The physics of thermocline ventilation. *Coupled Ocean–Atmosphere Models*, J. C. J. Nihoul, Ed., Elsevier Science, 543–590..

Worthington, L. V., 1959: The 18°C water in the Sargasso Sea. *Deep-Sea Res.*, **5**, 297–305..

Yasuda, T., and K. Hanawa, 1997: Decadal changes in the mode waters in the midlatitude North Pacific. *J. Phys. Oceanogr.*, **27**, 858–870.. [Find this article online](#)

Yuan, X., and L. D. Talley, 1992: Shallow salinity minima in the North Pacific. *J. Phys. Oceanogr.*, **22**, 1302–1316.. [Find this article online](#)

—, and —, 1996: The subarctic frontal zone in the North Pacific: Characteristics of frontal structure from climatological data and synoptic surveys. *J. Geophys. Res.*, **101**, 16 491–16 508..

Zhang, R.-H., and S. Levitus, 1997: Structure and cycle of decadal variability of upper-ocean temperature in the North Pacific. *J. Climate*, **10**, 710–727.. [Find this article online](#)

—, L. M. Rothstein, and A. J. Busalacchi, 1998: Origin of upper-ocean warming and El Niño change on decadal scales in the tropical Pacific Ocean. *Nature*, **391**, 879–883..

---

## Tables

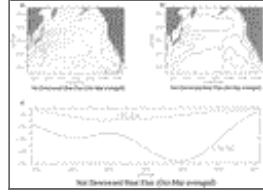
Table 1. Summary of model results along 140.5°W. Depth in meters.

	Control run	Run 1a (28.5°N stratification)	Run 2a (42.5°N stratification)	Run 3a (constructed stratification)
Minimum MLD (occurs at 46.5°N)	68.2	51.7	67.7	79.9
Maximum MLD (occurs at 28.5°N)	145.5	102.7	112.8	138.8
Mean MLD	125.6	122.0	98.3	132.6
Range (max – min)	177.3	51.0	45.1	58.9

[Click on thumbnail for full-sized image.](#)

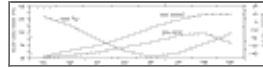
Table 2. Summary of model results along 179.5°E. Depth in meters.

## Figures



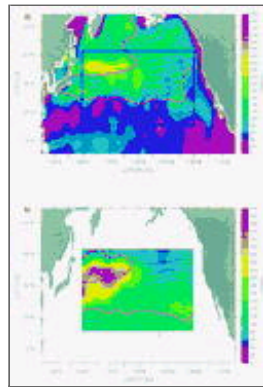
[Click on thumbnail for full-sized image.](#)

Fig. 1. Net downward heat flux from [da Silva et al. \(1994\)](#) (a) averaged over winter cooling season of Oct–Mar (contour interval:  $25 \text{ W m}^{-2}$ ), (b) averaged over summer warming season of Jul–Sep (contour interval:  $25 \text{ W m}^{-2}$ ), and (c) two meridional sections ( $140.5^\circ\text{W}$  and  $179^\circ\text{E}$ ) averaged over Oct–Mar (in  $\text{W m}^{-2}$ ).



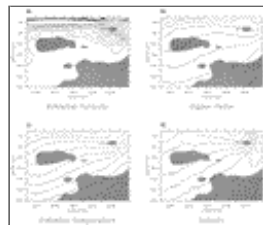
[Click on thumbnail for full-sized image.](#)

Fig. 2. Seasonal cycle (averaged along  $28.5^\circ\text{N}$ ,  $149.5^\circ\text{E}$ – $130.5^\circ\text{W}$ ) of net heat flux from [da Silva et al. \(1994\)](#), mixed layer depth calculated from the World Ocean Atlas 1994, and mixed layer depth calculated by the model.



[Click on thumbnail for full-sized image.](#)

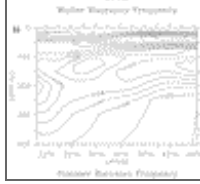
Fig. 3. March mixed layer depth (color; in meters) and sea surface temperature (black contours; contour interval:  $2^\circ\text{C}$ ). Red contours show Mar outcrops of the  $\sigma_\theta = 26.25$  and  $25.0 \text{ kg m}^{-3}$  surfaces. Mixed layer depth is defined as the depth at which  $\sigma_\theta$  is  $0.125 \text{ kg m}^{-3}$  different from the sea surface. (a) Calculated from the World Ocean Atlas 1994. The black box illustrates the model domain. (b) Calculated from the model.



[Click on thumbnail for full-sized image.](#)

Fig. 4. Annual-mean climatological sections along  $29.5^\circ\text{N}$  derived from the World Ocean Atlas 1994. Local PV minima discussed in the text are shaded. (a) Potential vorticity (contour interval:  $1 \times 10^{-10} \text{ m}^{-1} \text{ s}^{-1}$ ). Contours larger than  $10 \times 10^{-10} \text{ m}^{-1} \text{ s}^{-1}$  are not displayed. (b)  $\sigma_\theta$  (contour interval:  $0.5 \text{ kg m}^{-3}$ ). (c) Potential temperature (contour interval:  $2^\circ\text{C}$ ). (d) Salinity (contour interval:  $0.2 \text{ psu}$ ).





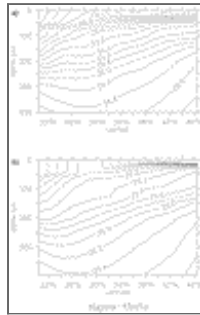
[Click on thumbnail for full-sized image.](#)

Fig. 5. Climatological buoyancy frequency calculated from the World Ocean Atlas 1994 along 140.5°W (contour interval: 0.001 s<sup>-1</sup>) (a) averaged over Jan–Mar and (b) averaged over Jul–Sep.



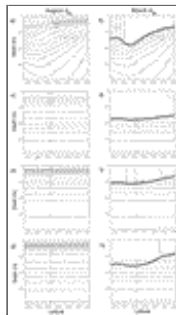
[Click on thumbnail for full-sized image.](#)

Fig. 6. Magnitude of the vertical maximum of the buoyancy frequency (s<sup>-1</sup>) in the upper 400 m in October calculated from the World Ocean Atlas 1994.



[Click on thumbnail for full-sized image.](#)

Fig. 7. August  $\sigma_\theta$  along 140.5°W (contour interval = 0.2 kg m<sup>-3</sup>). (a) Calculated from the World Ocean Atlas 1994. (b) Resulting from the model run discussed in the text.



[Click on thumbnail for full-sized image.](#)

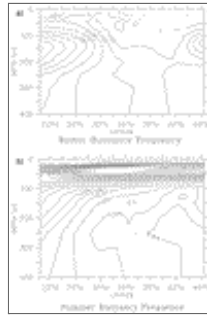
Fig. 8. Plot of  $\sigma_\theta$  along 140.5°W (contour interval: 0.2). The left column [(a), (c), (e), and (g)] shows the initial August conditions used for the control run (a)–(b), run 1a (c)–(d), run 2a (e)–(f), and run 3a (g)–(h). The right column [(b), (d), (f), and (h)] shows the resulting Mar density fields. The bold line shows mixed layer depth (defined as the depth at which  $\sigma_\theta$  is 0.125 kg m<sup>-3</sup> different from the sea surface).





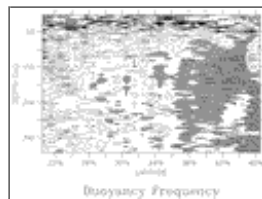
[Click on thumbnail for full-sized image.](#)

Fig. 9. Profiles of initial buoyancy frequency (in  $s^{-1}$ ) for the three test runs (solid: run 1a; dashed: 2a; and dashed-dotted: 3a).



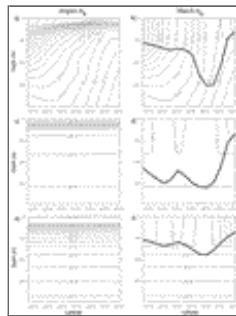
[Click on thumbnail for full-sized image.](#)

Fig. 10. Climatological buoyancy frequency calculated from the World Ocean Atlas 1994 along  $179.5^{\circ}\text{E}$  (contour interval =  $0.001 s^{-1}$ ) (a) averaged over Jan–Mar and (b) averaged over Jul–Sep.



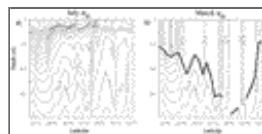
[Click on thumbnail for full-sized image.](#)

Fig. 11. Buoyancy frequency calculated from WOCE P14N data along  $179^{\circ}\text{E}$  in July 1993 (contour interval:  $0.002 s^{-1}$ ). Buoyancy frequencies  $<0.004 s^{-1}$  are shaded.



[Click on thumbnail for full-sized image.](#)

Fig. 12. Plot of  $\sigma_{\theta}$  along  $179.5^{\circ}\text{E}$  (contour interval:  $0.2 \text{ kg m}^{-3}$ ). The left column [(a), (c), and (e)] shows the initial August conditions used for the control run (a)–(b), run 1b (c)–(d), and run 2b (e)–(f). The right column [(b), (d), and (f)] shows the resulting Mar density fields. The bold line shows mixed layer depth (defined as the depth at which  $\sigma_{\theta}$  is  $0.125 \text{ kg m}^{-3}$  different from the sea surface).



[Click on thumbnail for full-sized image.](#)

Fig. 13. Plot of  $\sigma_{\theta}$  along  $179^{\circ}\text{E}$  (contour interval:  $0.2 \text{ kg m}^{-3}$ ) (a) from WOCE P14N data in Jul 1993 and (b) resulting Mar density field from model run that was initialized with WOCE P14N data. The bold line shows mixed layer depth (defined as the depth at which  $\sigma_{\theta}$  is  $0.125 \text{ kg m}^{-3}$  different from the sea surface).

Corresponding author address: Ms. Carol Ladd, School of Oceanography, University of Washington, Box 357940, Seattle, WA 98195-7940.

E-mail: [cladd@ocean.washington.edu](mailto:cladd@ocean.washington.edu)

top ▲



© 2008 American Meteorological Society [Privacy Policy and Disclaimer](#)

Headquarters: 45 Beacon Street Boston, MA 02108-3693

DC Office: 1120 G Street, NW, Suite 800 Washington DC, 20005-3826

[amsinfo@ametsoc.org](mailto:amsinfo@ametsoc.org) Phone: 617-227-2425 Fax: 617-742-8718

[Allen Press, Inc.](#) assists in the online publication of *AMS* journals.